Designing polar textures with ultrafast neuromorphic features from atomistic simulations

Sergey Prosandeev, Sergei Prokhorenko, Yousra Nahas, Yali Yang, Changsong Xu, Julie Grollier, Diyar Talbayev, Brahim Dkhil, L Bellaiche

Designing polar textures with ultrafast neuromorphic features from atomistic simulations

NEUROMORPHIC
Computing and Engineering

OPEN ACCESS

RECEIVED
28 November 2022

REVISED
16 January 2023

ACCEPTED FOR PUBLICATION
28 February 2023

PUBLISHED
15 March 2023

TOPICAL REVIEW

Designing polar textures with ultrafast neuromorphic features from atomistic simulations

Sergey Prosandeev[1,*], Sergei Prokhorenko[1], Yousra Nahas[1], Yali Yang[2], Changsong Xu[3,4], Julie Grollier[5], Diyar Talbayev[6], Brahim Dkhil[7] and L Bellaiche[1]

[1] Physics Department and Institute for Nanoscience and Engineering, University of Arkansas, Fayetteville, AR 72701, United States of America
[2] School of Mathematics and Physics, University of Science and Technology Beijing, Beijing 100083, People's Republic of China
[3] Key Laboratory of Computational Physical Sciences (Ministry of Education), Institute of Computational Physical Sciences, State Key Laboratory of Surface Physics, and Department of Physics, Fudan University, Shanghai 200433, People's Republic of China
[4] Shanghai Qi Zhi Institute, Shanghai 200030, People's Republic of China
[5] Unité Mixte de Physique, CNRS, Thales, Université Paris-Saclay, 91767 Palaiseau, France
[6] Department of Physics and Engineering Physics, Tulane University, 6400 Freret St., New Orleans, LA 70118, United States of America
[7] Université Paris-Saclay, CentraleSupélec, CNRS-UMR8580, Laboratoire Structures, Propriétés et Modélisation des Solides, 91190 Gif-sur-Yvette, France
[*] Author to whom any correspondence should be addressed.

E-mail: sprossan@uark.edu

Keywords: atomistic, simulations, ferroelectric, THz pulses, neuromorphic computing

Abstract

This review summarizes recent works, all using a specific atomistic approach, that predict and explain the occurrence of key features for neuromorphic computing in three archetypical dipolar materials, when they are subject to THz excitations. The main ideas behind such atomistic approach are provided, and illustration of model relaxor ferroelectrics, antiferroelectrics, and normal ferroelectrics are given, highlighting the important potential of polar materials as candidates for neuromorphic computing. Some peculiar emphases are made in this Review, such as the connection between neuromorphic features and percolation theory, local minima in energy path, topological transitions and/or anharmonic oscillator model, depending on the material under investigation. By considering three different and main polar material families, this work provides a complete and innovative toolbox for designing polar-based neuromorphic systems.

1. Introduction

It is known that our brain is an electrochemical device passing an enormous number of electrical signals by means of neurons. These latter communicate with neighboring neurons emitting a so called 'electric action potential': the connectors between the neurons, that are the synapses, 'recognize the purpose' of each action potential and respond via the stimulation or suppression of the transmission of a corresponding 'electrical or chemical message' to the nearest neurons or to the muscles [1].

There are many different models trying to understand and reproduce the behaviors of the neurons. Most of them are of 'Integrate-and-fire' type. The main idea is the integration of the electric signal in time, until the threshold value of the potential is reached. Then, the signal is passed farther out, that is 'the signal is fired' [2]. Depending on the repeatability of the signals reaching the synapse, the strength or weight of the synapse either reinforces or weakens, allowing learning-forgetting processes. This property is also called synaptic plasticity [3].

It is appealing to find non-alive matters possessing similar properties as neurons and synapses, and to then use these systems for machine learning purposes and multifunctional applications—where the neuronic 'Integrate-and-fire' model can be applied, e.g. to solid state materials. Such systems serve for 'Neuromorphic Architecture' and permit in-memory or 'Neuromorphic Computing' [4], which reduces energy consumption by avoiding continuous back and forth between the processing unit and the memory as it is currently the case in today's computers.

In this review, we present three different model polar compounds that, according to our large-scale atomistic simulations, exhibit neuromorphic signatures, when subject to THz electric pulses [5–7]. The first polar system is lead-magnesium-niobate ($Pb(Mg_{1/3}Nb_{2/3})O_3$, denoted as PMN), which is a representative of relaxor ferroelectrics which are characterized by intrinsic short-correlated dipolar textures, the so-called polar nanoregions [8–10]. Consequently, its ground state is non-ferroelectric, likely partly due to the off-centering of lead-ions and random electric fields caused by the magnesium and niobium ions that have different chemical charges and that occupy the B-sublattice of the ABO_3 perovskite structure [11]. Nevertheless, when subject to *dc* electric fields, PMN, which average total polarization is zero, undergoes a first-order phase transition and becomes ferroelectric with a long-range polar order and non-zero polarization [12]. We will emphasize here that, in fact, it is also possible to induce different values of the polarization by achieving different and so-called hidden states the material can experience, by applying THz electric pulses. Note that the hidden states are intrinsically metastable and cannot be reached under equilibrium conditions. They have been found in superconductors [13], colossal magnetoresistance manganites [14], charge density wave materials [15], and incipient ferroelectrics [16, 17]. Such states were also found [5, 6] to have properties distinct from those of the thermodynamically stable ground state in relaxors.

The second example is sodium niobate, $NaNbO_3$ (NNO), which is a representative of room-temperature antiferroelectric materials [18], which are the counterpart of ferroelectrics characterized by antipolar texture arrangements that can be altered by electric fields.

Finally, the third type of the polar materials is a classical ferroelectric system and, more specifically, ultrathin films made of lead-zirconium-titanate, $PbZr_{1-x}Ti_xO_3$ (PZT). 'Normal' ferroelectrics have already been exploited for neuromorphic functionalities by considering the tunability of the ratio between up and down ferroelectric domains under electric field pulses [19]. Here, we rather exploit their ability to exhibit a variety of exotic polar textures, such as stripe-like dipole pattern, vortices, bubble, skyrmions, etc, depending on electrical and mechanical boundary conditions [20].

It is also important to realize that the THz frequency of the electrical signals we use in the simulations for these three families of polar compounds is much larger than the frequency used in the brain, which ranges from 0.5 to 42 Hz [21], but also than the GHz frequency typically used for other neuromorphic materials—such as magnetic-based ones [22], memristive and nanoionic devices [23], and phase change materials [24]. This also automatically implies that our predictions can be important for applications significantly enhancing the speed of neuromorphic solid-state-based devices, that is to design ultrafast neuromorphic computing. Such ultrafast devices can enhance works on machine learning [25, 26] and they can have low energy consumption if the transformations under the pulse are nonvolatile. Enabling tunable and multiple polar non-volatile states or weighted inputs, having the ability of temporal integration of the polarization, permitting thresholding for signal spiking and resetting the polarization are among the requested features to achieve neuronic and synaptic functions allowing implementation of polar materials in neuromorphic computing. Because today's needs in artificial intelligence require real-time data processing, and thus higher speeds, the computing systems based on neuromorphic electronic processors have reached some limits as the process information can only be done up to MHz speeds. In parallel to the development of crossbar architectures allowing to increase the speed [27, 28], and in order to face neuromorphic electronic system issues that limit fast operation speeds (crosstalk, parasitic capacitance, Joule-heating to cite a few), it is necessary to look for alternatives such as photonic light-based systems (see [29, 30] and references therein), or in other words to go towards higher frequency ultrafast computing. This has been recently considered in various materials, e.g. quantum semiconductors [31], resistive switching systems [32], phase change materials [33] or magnetic-based materials [34] to name a few, in a frequency ranging from GHz to THz. Note that the speeds for neuronic and synaptic functions are directly linked to the material-related mechanisms. It is interesting to stress here that THz frequencies are typical frequencies of optical phonons that trigger and drive the polarization in ferroelectrics and related materials, and, hence, polar compounds and their ultrafast switching dynamics are promising for THz neuromorphic computing.

This review is organized as follows. Section 2 provides some details about the numerical scheme used in the three aforementioned studies [5–7]. Sections 3–5 present and emphasize some results of such scheme for PMN, NNO and PZT systems, respectively. Section 6 summarizes this article.

2. Methods

The computational technique employed is the effective Hamiltonian scheme [35–37]. Conceptually, this method relies on four pillar ideas. First of all, one has to select the few degrees of freedom that are relevant to the material and phenomena to be investigated. They are typically the local soft mode on the 5-atom cell j, $\mathbf{u}_j$, which is proportional to the electric dipole moment of such cell and which is constructed following [35]; the

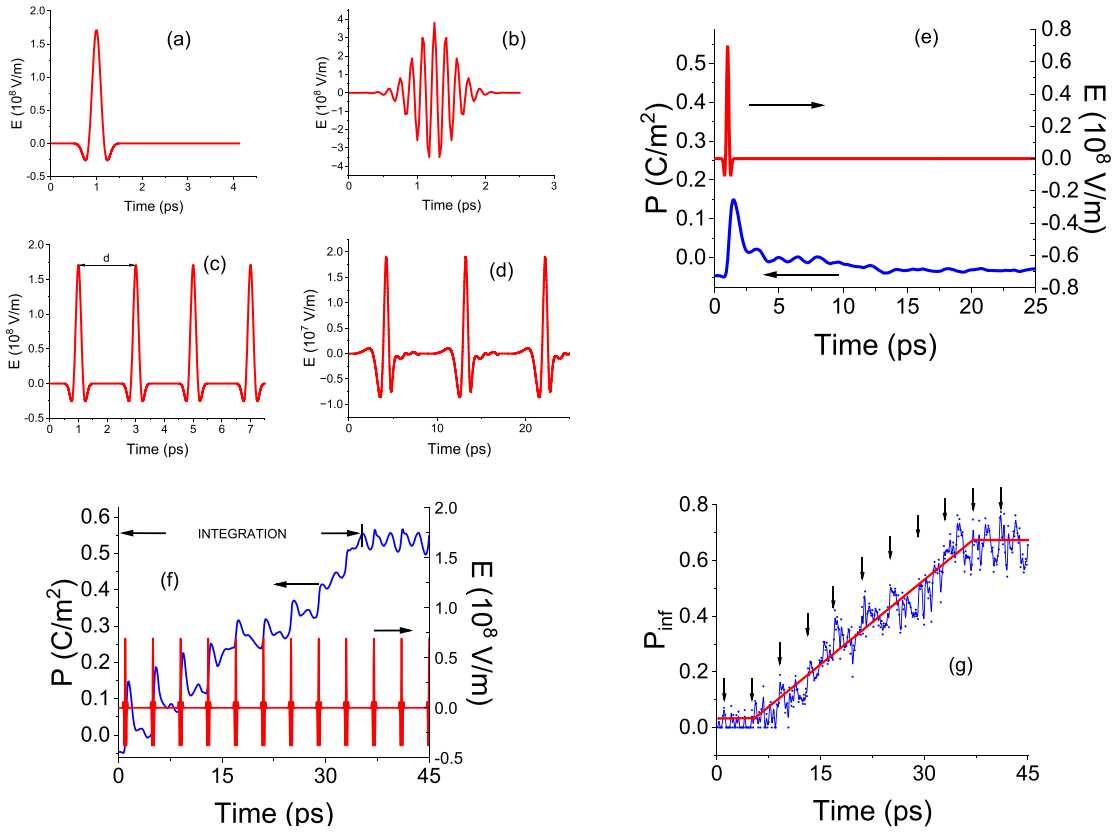

Figure 1. (a) A single electric pulse used. Reprinted figure with permission from [5], Copyright (2021) by the American Physical Society. (b) A single electric pulse used. Reprinted figure with permission from [6], Copyright (2022) by the American Physical Society. (c) A train made of electric pulses used. Reprinted figure with permission from [5], Copyright (2021) by the American Physical Society. (d) A train made of the electric pulses experimentally generated. Reprinted figure with permission from [39], Copyright (2018) by the American Physical Society. (e) Response of the electrical polarization of PMN when the single electric pulse shown in red. Reprinted figure with permission from [5], Copyright (2021) by the American Physical Society. (f) When under the train of electric pulses also displayed in red. Reprinted figure with permission from [5], Copyright (2021) by the American Physical Society. (g) Percolation cluster strength as a function of time for the same train of pulses as in panel (c), with the arrows showing the positions of these pulses. Reprinted figure with permission from [5], Copyright (2021) by the American Physical Society.

homogeneous strain, η_μ, where the $\mu = 1-6$ indices are used in line with Voigt's notations [38], as well as, inhomogeneous strain that is characterized by an on-site vector v_j for each 5-atom cell j; and, for the case of NNO, a pseudo-vector $\boldsymbol{\omega}_j$, whose direction is the axis about which the oxygen octahedron of cell j rotates about and whose magnitude is the angle of this rotation. Secondly, one derives, based on symmetry, the analytical expression of the most important and low-order energetic terms involving these degrees of freedom as well as their couplings. Thirdly, the parameters quantifying the strength of such terms are then derived from first-principle calculations on small cells [36]. Fourthly and finally, molecular dynamics (MD) simulations are conducted on relatively large supercells, namely $18 \times 18 \times 18$ in [5] and $12 \times 12 \times 12$ in [6, 7], using these degrees of freedom, analytical expressions and parameters, in order to obtain time-dependent quantities at finite temperature. It is important to further know that these simulations also incorporate the influence of an electric field on physical properties by simply adding, within the effective Hamiltonian method, an energy $-Z^* \sum_i \mathbf{u}_i \cdot \mathbf{E}$, where $\mathbf{E}$ is the electric field, $\mathbf{u_i}$ the local mode at each site i, and Z^* the dynamical charge of the local mode. For all calculations conducted in our three aforementioned studies about neuromorphic computing, the electric field associated with each pulse typically has the following form:

$$\mathbf{E}_p(t) = \mathbf{E}_0 exp\left[-\frac{(t-t_0)^2}{\delta^2}\right] cos\left[\omega(t-t_0)\right]. \quad (1)$$

This pulse is therefore a product of Gaussian and cosine functions. Figures 1(a) and (b) present one such pulse with different ω ($\nu = 1.5$ and 6 THz, respectively), and figure 1(c) shows a train of these pulses separated in time by the interval d ($\nu = 1.5$ THz, $d = 2$ ps). For comparison, in figure 1(d), we show a train of pulses realized in experiments of [39]. See supplement material to [5] for the study of the dependence of the shape of the pulses on the shape of the polarization response.

3. Lead-magnesium-niobate: role of percolation theory in the formation of hidden states

Let us start with some results on PMN [5]. For the parameters of equation (1), we use the following values: $\mathbf{E}_0$ is oriented along the [111] direction and its magnitude is $4\sqrt{3} \times 10^7$ V m^{-1}, $\delta = 0.2$ ps, and $\nu = \omega/2\pi = 1.5$ THz.

Figure 1(e) reports the temporal behavior of the polarization (shown in blue) when only one electric pulse is applied (this single pulse is displayed in red in figure 1(a)). One can see that the initially non-polar PMN (in its initial relaxor state) responds to this single pulse by developing a polarization, the peak of which is shifted from the peak of the electric field by about 0.5 ps, and then slowly relaxes when the pulse has died out (see also [16, 40] for a similar shift found in $SrTiO_3$ at low temperatures). So, the shape of the polarization response is not the same as the shape of the electric signal. One may wonder why there is a time delay between the peaks of the polarization and the electric field. We will discuss this point in section 4 via the introduction of a simple model.

Figure 1(f) shows the result of the polarization in PMN when now subject to a train of the electric pulses that are separated by 4 ps. Consecutive electric pulses result in a consecutive pumping of the polarization, that is PMN transitions to different hidden states having progressively increased value of the polarization until reaching a final ferroelectric state with a rather large polarization. This behavior can be related to the integration process inherent to neuromorphic materials. Interestingly, we numerically found that all of these intermediate states are metastable, in the sense that PMN gets stuck in them when we switch off the field just after the times these hidden states have been reached. The fact that these multiple states are metastable and thus non-volatile states, allows to consider them as multi-weights, that one can exploit in artificial neuromorphic synapses. We also numerically discovered that these hidden states microscopically correspond to the growth of some polar nanoregions having a local polarization lying along the field's direction, until such clusters percolate to give rise to the final ferroelectric state of R3m symmetry. The relevance of the percolation theory for PMN under electric pulses is demonstrated in figure 1(g) that presents the calculated strength of the so-called infinite percolation cluster P_{inf} as a function of time, when the same train of THz pulses as that shown in figure 1(c) is applied. As a matter of fact, figure 1(g) reveals that P_{inf} starts from zero, then increases after each pulse occurs and then reaches and fluctuates around a significant finite value, of about 0.55 C m^{-2}, once PMN attains its final ferroelectric phase. The percolation cluster involves dipoles satisfying the following condition: for each nearest neighbor pair, the direction of two dipoles can differ by no more than 10%, and the cluster possessing such dipoles is said to be a percolation cluster only if spreads from one boundary of the supercell to the opposite one, and so in all three Cartesian directions. The strength of the percolation cluster is the ratio of the unit cells belonging to this cluster to the total number of the unit cells in the supercell. Note that, in PMN, this ratio does not reach its maximal value of one in the ferroelectric phase, because of the inherent local disorder (mostly due to random fields arising from the fact that Mg and Nb ions do not belong to the same column of the periodic table).

4. Sodium niobate: homogeneous hidden states and energy paths

Let us now focus on $NaNbO_3$ bulk at 100 K and subject to a train of pulses equally separated by a time of 8 ps and given by equation (1) (this time is chosen such as to allow NNO bulk to relax within the reached hidden states after each pulse is applied and died out), with the field being applied along the pseudo-cubic [111] direction, E_0 having a magnitude of $2.2\sqrt{3} \times 10^8$ V m^{-1}, $\delta = 0.4$ ps, and $\nu = \omega/2\pi = 6$ THz [6]. It is important to know that we numerically found that NNO does not precisely possess for some temperatures the (antiferroelectric) orthorhombic Pbcm symmetry but rather an orthorhombic $Pca2_1$ space group that is deduced from Pbcm by adding a rather small polarization along the pseudo-cubic [001] direction [41].

Figure 2 shows the resulting temporal evolution of the component of the polarization along the pseudo-cubic [111] direction of $NaNbO_3$ bulk. As for the case of PMN, electric pulses successively applied to the initial state ($Pca2_1$ phase, here) provoke a polarization pumping and transitions to hidden states of increasing polarization, until a final ferroelectric state is reached (this final state in NNO bulks has a R3c symmetry and presents both a significant value of the electrical polarization along the pseudo-cubic [111] direction and antiphase tiltings about that axis). These hidden states also distinguish themselves by jumps in values of some oxygen octahedra tiltings and antipolar displacements (not shown here), and are found to be metastable—that is they persist when switching off the field once they are reached by the application of the THz pulses.

In order to understand the main reason for the existence of these intermediate hidden states, we turned to direct first-principle methods and employed the elastic-band method [42] implemented in the Vienna *ab-initio* package [43]. This method finds the most energy sustainable path between two different phases of matter, in our case $Pca2_1$ for the initial state and R3c for the final phase.

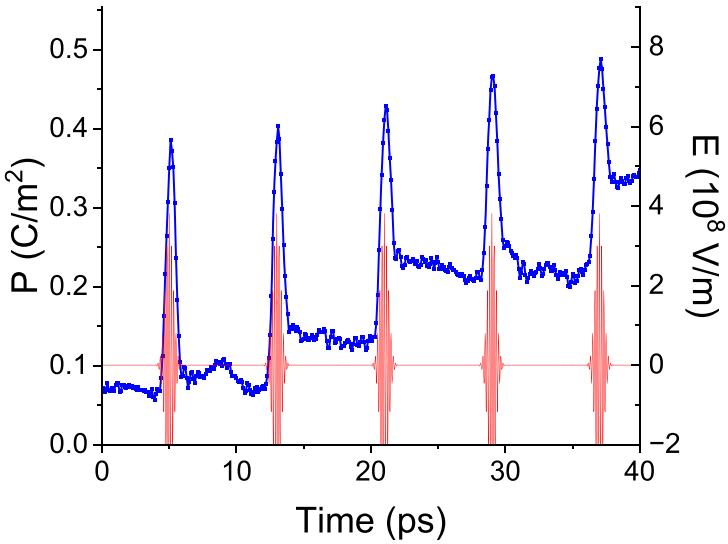

Figure 2. Time-development of the component of the polarization along the pseudo-cubic [111] direction (displayed by the blue line) under our chosen electric field pulses (shown by the red line). Reprinted figure with permission from [6], Copyright (2022) by the American Physical Society.

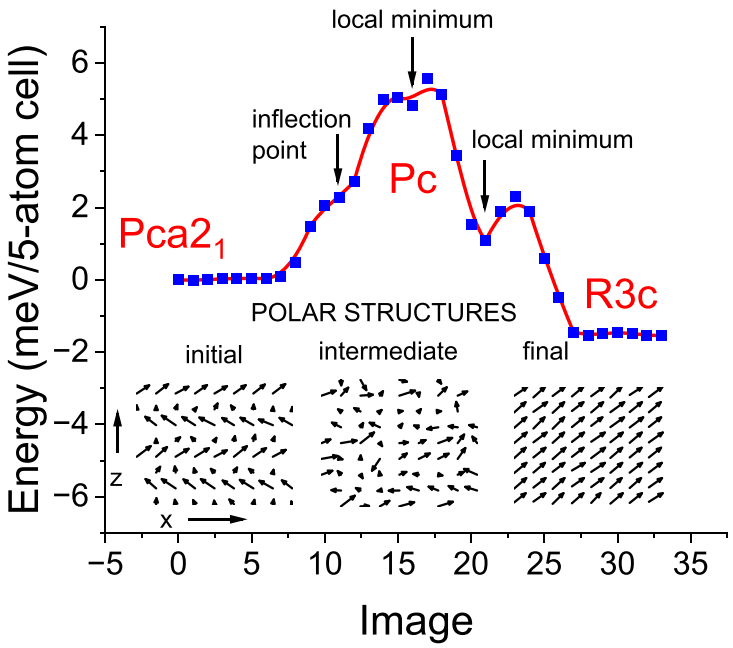

Figure 3. Energy path between $Pca2_1$ and R3c phases of NNO bulk, as found from *ab-initio* calculations employing the elastic-band method (see supplement to [6]). The snapshots at the bottom of the graph visualize the dipole polar order in the end-point and intermediate phases. The intermediate phase corresponds to the local minimum at the top of the path. Reprinted figure with permission from [6], Copyright (2022) by the American Physical Society.

Figure 3 presents such first-principles-calculated path for NNO bulk. One can see that this path contains a maximum in energy, which corresponds to the barrier one has to climb to go from $Pca2_1$ to R3c, but also possesses some local minima or inflection points, that are precisely the aforementioned hidden states. These latter are of Pc symmetry and are homogeneous in nature, unlike the intermediate hidden phases found for PMN. The snapshots show a gradual evolution of the polar structure from mostly antipolar to strong ferroelectric structure.

In other words, the hidden states can have different characters depending on the system under investigation. Note that we also employed the elastic-band method but within the Effective Hamiltonian method and found qualitatively similar results for the intermediate hidden states of NNO bulk (see [6] for that).

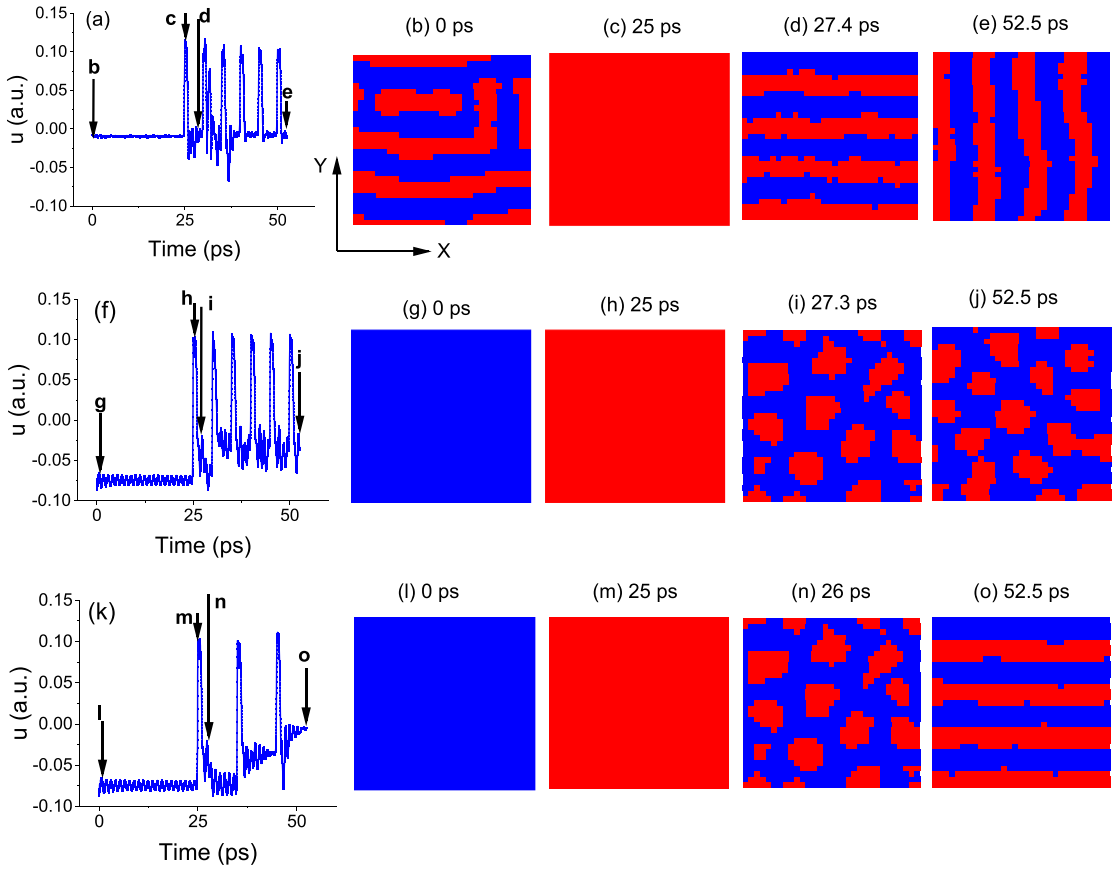

Figure 4. Time-development of the local mode (the blue line) under electric field pulses being along the pseudo-cubic [001] direction in the three cases described in the text: Case 1 (a), Case 2 (f), and Case 3 (k) [7]. In each case, the snapshots at different times are shown in the *XY* plane that is located at the middle of the film. The red and blue colors in these snapshots mark up- and down- domains correspondingly. (a)–(o) [7] John Wiley & Sons. [© 2022 Wiley-VCH GmbH].

5. Lead-zirconium-titanate: topological changes under electric pulses in a normal ferroelectric system

Let us now pay attention to PZT ultrathin films under a train of electric pulses at 10 K [7]. The parameters of equation (1) for the pulses are the following: the field is oriented along the pseudo-cubic [001] direction, $E_0 = 5 \times 10^8$ V m^{-1}, $\delta = 0.4$ ps, and $\nu = \omega/2\pi = 2$ THz in equation (1). The time-interval between successive pulses is either chosen to be 5 ps or 10 ps. The film is 5 layers-thick, is under a misfit epitaxial strain of −2.65% and has a Ti composition of 60%. The Zr and Ti ions are randomly distributed within the B-sublattice of the ABO_3 perovskite structure, therefore mimicking a chemically disordered ultrathin film. We also choose a specific and realistic electrical boundary condition that corresponds to 87% of screening of polarization-induced surface charges (this screening is represented by the symbol β, that is we have here $\beta = 0.87$). Such electrical boundary condition, along with the chosen mechanical one, leads to the so-called nanostripe ground state wherein the 'up' and 'down' polarized regions are separated by polarization vortex tubes. Notably, the material can also adopt a glass-like version of nanostripes commonly called the polar labyrinths [44]. The energy of such labyrinth patterns is very close to that of the ground state. We further investigated three cases. Case 1 corresponds to the initial state being a labyrinthine pattern and PZT being under a train of pulses that are separated by 5 ps; Case 2 is associated with the same train of pulses but the initial state is now a polar monodomain with a polarization oriented along $[00\bar{1}]$; Case 3 has the same initial state than Case 2 but with the time difference between the successive pulses having now increased by two times with respect to Case 2. The temporal dependence of the polarization along the [001] direction is shown in figures 4(a), (f) and (k) for Cases 1–3, respectively. The other panels of figure 4 display the textures of the local electric dipoles about 25 ps before the first pulse, during the first pulse, just after the first pulse, and after the last pulse.

One can see that, once again, different hidden states can be reached when applying a train of THz pulses. For instance, in Case 1, the initial labyrinth texture transforms first to a monodomain with a polarization along [001] after the first pulse and then to different textures including nanostripes that can alternate along

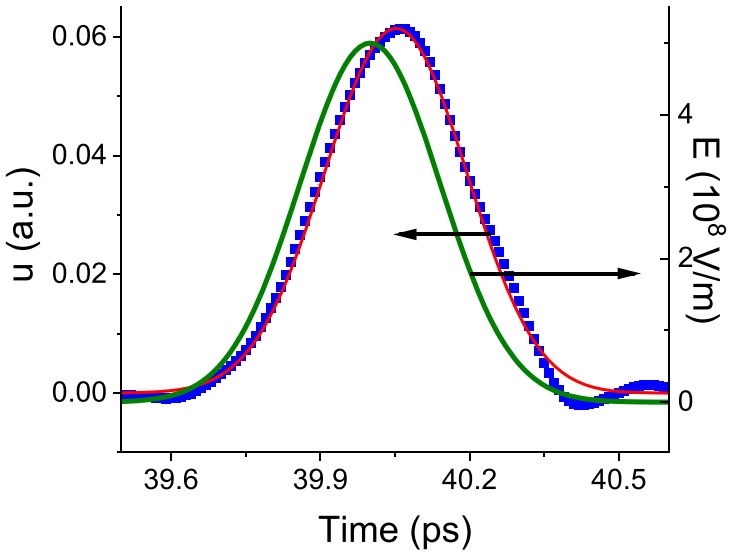

Figure 5. MD data (in blue) and its fit by the proposed anharmonic oscillator model (in red) for the response of the local mode to the electric pulse shown in green. [7] John Wiley & Sons. [© 2022 Wiley-VCH GmbH].

different directions. In Case 2, the initial monodomain with a polarization along $[00\bar{1}]$ transforms to a monodomain with opposite polarization during the first pulse, and, then, many bubble states are reached. One difference between Case 3 and Case 2 is that the former adopts nanostripes at the end of the application of the pulses while the latter exhibits a bubbles state. We further found that the final states for Cases 1–3 remain the same when allowing the simulations to continue but under no pulses, which demonstrate their stable and/or metastable character. It is important to realize that nanostripes, labyrinths and bubbles are topological in nature, implying that topology can also play a role in neuromorphic materials.

In order to deepen the knowledge of neuromorphic materials, it is also important to be able to mimic the behavior of the electrical polarization under a THz pulse. For that, we developed in [7] an anharmonic oscillator model that involves the local mode u and that depends on the bare frequency ω_{HO}, damping constant γ, the electric field $E(t)$ associated with the pulse, and a b constant characterizing the nonlinearity of the dependence of u on E. More precisely, the differential equation describing the dynamics of this oscillator has the form:

$$\ddot{u} + \gamma\dot{u} + \omega_{HO}^2 u + bu^3 = \frac{Z^* E(t)}{m}, \tag{2}$$

where m is the oscillator's mass, and dots on top of symbols represent time derivatives. The specific solution of equation (2) can be expressed as [45]:

$$\begin{aligned} u(t,\Omega,\gamma) &= \frac{Z^*}{m\Omega}\int_0^t dt' e^{-\gamma(t-t')} E(t') \sin\left[\Omega(t-t')\right] \\ &= A\int_0^t dt' e^{-\gamma(t-t')} E(t') \sin\left[\Omega(t-t')\right], \end{aligned} \tag{3}$$

where $\Omega^2 = \omega_{HO}^2 - \gamma^2 + bu^2$ and $A = Z^*/m\Omega$. Note that, at negative Ω^2, the sine function in equation (3) above becomes the sine hyperbolic function (we will show the difference between the underdamped and overdamped cases elsewhere).

Let us check if this model can reproduce well our MD data, and picked the case of $\beta = 0.8$ for PZT ultrathin films for that. Figure 5 demonstrates that the MD data for the supercell average of the local mode for $\beta = 0.8$ can indeed be fitted rather well by equation (3) with a vanishing nonlinear b coefficient in that case ($\omega_{HO} = 4.545$ THz and $\gamma = 3.205$ THz). In fact, we numerically found that such equation reproduces rather well cases for other β's, but with the b coefficient becoming non-zero and the ω_{HO} frequency significantly reducing its value when approaching the critical β of 0.86–0.87 at which a transition from nanostripes to monodomain occurs for the ground state. It is important to know that this model can result in a time delay between the peak of the polarization and that of the electric field, with the Ω and γ parameters governing this time delay.

6. Summary

In summary, we used effective Hamiltonian techniques to search for, and understand, materials for neuromorphic functionalities [5–7]. Let us emphasize the following achievements done in [5–7] and summarized in the present review:

1. We predicted that the prototype of relaxor ferroelectrics, that is PMN, can exhibit the three main features of neuromorphic materials, that are action potentials, integration and multiple states (of varying polarization here), when under THz electric pulses. The connection between these latter (hidden) states, percolation theory and growth of polar nanoregions (PNRs) was also established [5].
2. We also numerically found that one well-known antiferroelectric system, namely NNO bulk, is also promising for being an active player in ultrafast neuromorphic architecture. One major difference between NNO and PMN is that the hidden states are homogeneous in nature in the former while being strongly inhomogeneous (due to the PNRs) in the latter. Determining the structural path joining the initial antiferoelectric-like initial state to the final strongly ferroelectric phase, and finding local minima in this path, was essential to understand the occurrence of neuromorphic signatures in NNO [6].
3. We also revealed that hidden or even final states can be topological in nature in normal ferroelectrics, such as PZT ultra-thin films, under THz excitations. Note that some magnetic topological defects like skyrmion can also be useful for neuromorphic computing [46]. We also presented an anharmonic damped oscillator model reproducing and explaining how the electrical polarization can respond to such excitations [7].

All the materials indicated here, namely PMN, NNO, and PZT films, have in common that (i) they are complex systems with (ii) complicated energy landscape involving many states, some being mostly non-polar while others have intermediate or strong value of the polarization. Applying THz electric pulses to them allows these systems to explore such energy landscape via out-of-equilibrium processes. It may be also important that (iii) the applied field lies along the direction of the polarization of a strong ferroelectric state, e.g. along [111] for R3m in PMN and R3c in NNO *versus* [001] for the tetragonal monodomain of PZT. Such strategy of combining items (i)–(iii) may be used to design (and understand) novel neuromorphic materials. For instance, one may wonder if the solid solutions (Bi,R)FeO_3, where *R* is a rare-earth ion, can also present neuromorphic features since they can have different phases: a strong ferroelectric rhombohedral R3c state with a polarization oriented along [111], the 'typical' tilted, non-polar Pnma phase, but also unusual complex states with different polarization values and anomalous tilting patterns [7, 47–53].

Data availability statement

All data that support the findings of this study are included within the article (and any supplementary files).

Acknowledgments

Sergey P and L B thank an Impact grant from the Arkansas Research Alliance (ARA) and ONR Grant No. N00014-21-1-2086. Sergei P and L B acknowledge the Vannevar Bush Faculty Fellowship (VBFF) from the Department of Defense. Y N and L B thank the ARO Grant No. W911NF-21-1-0113. J G acknowledges support from Q-MEEN-C, an Energy Frontier Research Center funded by the U.S. Department of Energy (DOE), Office of Science, Basic Energy Sciences (BES), under Award No. DE-SC0019273, for work on neuromorphic computing with PZT. D T acknowledges support from NSF for the work on terahertz-driven ferroelectric dynamics under Grant No. DMR-1554866. B D thanks the European Union's Horizon 2020 research and innovation programme under Grant Agreement No. 964931 (TSAR). C X acknowledges financial support from the Ministry of Science and Technology of the People's Republic of China (No. 2022YFA1402901) and from NSFC (No. 12274082).

ORCID iD

Sergey Prosandeev https://orcid.org/0000-0002-0511-8310

References

[1] Kandel E R, Schwartz J H and Jessell T M 2000 *Principles of Neural Science* (New York: McGraw-Hill)
[2] Gerstner W and Kistler W M 2002 *Spiking Neuron Models: Single Neurons, Populations, Plasticity* (Cambridge: Cambridge University Press)

[3] Citri A and Malenka R C 2008 *Neuropsychopharmacology* **33** 18
[4] Ben Abdallah A and Dang K N 2022 *Neuromorphic Computing Principles and Organization* (Berlin: Springer)
[5] Prosandeev S, Grollier J, Talbayev D, Dkhil B and Bellaiche L 2021 *Phys. Rev. Lett.* **126** 027602
[6] Prosandeev S, Prokhorenko S, Nahas Y, Yang Y, Xu C, Grollier J, Talbayev D, Dkhil B and Bellaiche L 2022 *Phys. Rev.* B **105** L100101
[7] Prosandeev S, Prokhorenko S, Nahas Y, Grollier J, Talbayev D, Dkhil B and Bellaiche L 2022 *Adv. Electron. Mater.* **8** 202200808
[8] Smolenskii G A, Isupov V A, Agranovskaya A I and Popov S N 1961 *Sov. Phys. Solid State* **2** 2584
[9] Cross L E 1994 *Ferroelectrics* **151** 305
[10] Kleemann W 2006 *J. Mater. Sci.* **41** 129
[11] Al-Barakaty A, Prosandeev S, Wang D, Dkhil B and Bellaiche L 2015 *Phys. Rev.* B **91** 214117
[12] Colla E V, Koroleva E Y, Okuneva N M and Vakhrushev S B 1995 *Phys. Rev. Lett.* **74** 1681
[13] Fausti D, Tobey R I, Dean N, Kaiser S, Dienst A, Hoffmann M C, Pyon S, Takayama T, Takagi H and Cavalleri A 2011 *Science* **331** 189
[14] Rini M, Tobey R, Dean N, Itatani J, Tomioka Y, Tokura Y, Schoenlein R W and Cavalleri A 2007 *Nature* **449** 72
[15] Stojchevska L, Vaskivskyi I, Mertelj T, Kusar P, Svetin D, Brazovskii S and Mihailovic D 2014 *Science* **344** 177
[16] Li X, Qiu T, Zhang J, Baldini E, Lu J, Rappe A M and Nelson K A 2019 *Science* **364** 1079
[17] Nova T F, Disa A S, Fechner M and Cavalleri A 2019 *Science* **364** 1075
[18] Lines M E and Glass A M 1977 *Principles and Applications of Ferroelectrics and Related Materials* (Oxford: Clarendon)
[19] Wang S *et al* 2022 *Adv. Electron. Mater.* **9** 2200877
[20] Nahas Y, Prokhorenko S, Zhang Q, Govinden V, Valanoor N and Bellaiche L 2020 *Nat. Commun.* **11** 5779
[21] Klimesch W 2018 *Eur. J. Neurosci.* **48** 2431
[22] Locatelli N, Cros V and Grollier J 2014 *Nat. Mater.* **13** 11
[23] Sangwan V K and Hersam M C 2020 *Nat. Nanotechnol.* **15** 517
[24] Wang L, Lu S-R and Wen J 2017 *Nanoscale Res. Lett.* **12** 347
[25] Wang L, Lu S-R and Wen J 2017 *31st Conf. on Neural Information Processing Systems (NIPS) (Long Beach, CA)*
[26] Devlin J, Chang M-W, Lee K and Toutanova K 2019 *Proc. 2019 Conf. North American Chapter of the Association for Computational Linguistics: Human Language Technologies* vol 1 (Minneapolis, MN: Association for Computational Linguistics) p 4171
[27] Jung S *et al* 2022 *Nature* **601** 211
[28] Sebastian A, Le Gallo M, Khaddam-Aljameh R and Eleftheriou E 2020 *Nat. Nanotechnol.* **15** 529
[29] Robertson J, Kirkland P, Alanis J A, Hejda M, Bueno J, Di Caterina G and Hurtado A 2022 *Sci. Rep.* **12** 4874
[30] Zhu C *et al* 2022 *Light Sci. Appl.* **11** 337
[31] Sarantoglou G, Skontranis M and Mesaritakis C 2020 *IEEE J. Sel. Top. Quantum Electron.* **26** 1
[32] Zhou F *et al* 2019 *Nat. Nanotechnol.* **14** 776
[33] Chen X, Xue Y, Sun Y, Shen J, Song S, Zhu M, Song Z, Cheng Z and Zhou P 2022 *Adv. Mater.* 2203909
[34] Mitrofanova A, Safin A, Kravchenko O, Nikitov S and Kirilyuk A 2022 *Appl. Phys. Lett.* **120** 072402
[35] Zhong W, Vanderbilt D and Rabe K M 1995 *Phys. Rev.* B **52** 6301 Zhong W, Vanderbilt D and Rabe K M 1994 *Phys. Rev. Lett.* **73** 1861
[36] Bellaiche L, Garcia A and Vanderbilt D 2000 *Phys. Rev. Lett.* **84** 5427 Bellaiche L, Garcia A and Vanderbilt D 2002 *Ferroelectrics* **266** 41
[37] Bellaiche L and Vanderbilt D 2000 *Phys. Rev.* B **61** 7877
[38] Voigt W 1910 *Lehrbuch der Kristallphysik (mit Ausschluss der Kristalloptik)* (Leipzig: B. G. Teubner)
[39] Lin S, Yu S and Talbayev D 2018 *Phys. Rev. Appl.* **10** 044007
[40] Katayama I, Aoki H, Takeda J, Shimosato H, Ashida M, Kinjo R, Kawayama I, Tonouchi M, Nagai M and Tanaka K 2012 *Phys. Rev. Lett.* **108** 097401
[41] Yang Y, Xu B, Xu C, Ren W and Bellaiche L 2018 *Phys. Rev.* B **97** 174106
[42] Mills G, Jónsson H and Schenter G K 1995 *Surf. Sci.* **324** 305
Jónsson H, Mills G and Jacobsen K W 1998 *Classical and Quantum Dynamics in Condensed Phase Simulations* ed Berne B J, Ciccotti G and Coker D F (Singapore: World Scientific)
[43] Kresse G and Furthmüller J 1996 *Phys. Rev.* B **54** 11169
Kresse G and Furthmüller J 1996 *Comput. Mater. Sci.* **6** 15
Kresse G and Hafner J 1993 *Phys. Rev.* B **47** 558
[44] Nahas Y *et al* 2020 *Nature* **577** 47
[45] Hattori T 2010 *J. Chem. Phys.* **133** 204503
[46] Yokouchi T, Sugimoto S, Rana B, Seki S, Ogawa N, Shiomi Y, Kasai S and Otani Y 2022 *Sci. Adv.* **8** eabq5652
[47] Levin I, Karimi S, Provenzano V, Dennis C L, Wu H, Comyn T P, Stevenson T J, Smith R I and Reaney I M 2010 *Phys. Rev.* B **81** 020103(R)
[48] Levin I, Tucker M G, Wu H, Provenzano V, Dennis C L, Karimi S, Comyn T, Stevenson T, Smith R I and Reaney I M 2011 *Chem. Mater.* **23** 2166
[49] Xu B, Wang D, Íñiguez J and Bellaiche L 2015 *Adv. Funct. Mater.* **25** 552
[50] Chen J, Xu B, Liu X Q, Gao T T, Bellaiche L and Chen X M 2019 *Adv. Funct. Mater.* **29** 1806399
[51] Patel K, Prosandeev S, Xu B and Bellaiche L 2019 *Phys. Rev.* B **100** 214107
[52] Prosandeev S, Wang D, Ren W, Íñiguez J and Bellaiche L 2013 *Adv. Funct. Mater.* **23** 234
[53] Prosandeev S and Bellaiche L 2022 *Phys. Rev.* **6** 116201